SCIENCE CHINA
Information Sciences

• RESEARCH PAPER •

February 2021, Vol. 64 122402:1–122402:10
https://doi.org/10.1007/s11432-020-3005-8

Design space for stabilized negative capacitance in HfO_2 ferroelectric-dielectric stacks based on phase field simulation

Pengying CHANG, Gang DU & Xiaoyan LIU*

Institute of Microelectronics, Peking University, Beijing 100871*, China*

Received 8 May 2020/Revised 22 June 2020/Accepted 24 July 2020/Published online 20 January 2021

Abstract Polarization evolution with space and time in HfO_2 based metal-ferroelectric-insulator-metal (MFIM) structure is studied based on the phase field model by self-consistently solving the two-dimensional time-dependent Ginzburg-Landau and Poisson equations. Through examining the domain wall and electrostatic (depolarization) energies compared with the negative ferroelectric (FE) anisotropy energy, the correlation between the domain pattern (phase transition) and negative capacitance (NC) effect is revealed for different structure parameters and material properties, including FE thickness and gradient coefficient, dielectric permittivity and thickness, and operation frequency of applied voltage. The design space for stabilized NC with (near) hysteresis-free operation accompanied with voltage amplification is limited by phase transition, implying the potentials and limitations of FE HfO_2 for energy-efficient steep-slope devices.

Keywords ferroelectric, polarization dynamics, hysteresis, negative capacitance, depolarization field

Citation Chang P Y, Du G, Liu X Y. Design space for stabilized negative capacitance in HfO_2 ferroelectric-dielectric stacks based on phase field simulation. Sci China Inf Sci, 2021, 64(2): 122402, https://doi.org/10.1007/s11432-020-3005-8

1 Introduction

Ferroelectrics (FEs) have attracted great interests owing to their potentials in nonvolatile memories and steep-slope devices [1–3]. The recent advent of doped hafnium oxide HfO_2-based FEs has inspired researchers due to their good scalability and compatibility with standard CMOS technology compared with traditional perovskites [4–6]. Under this condition, negative-capacitance field effect transistors (NC-FETs) using HfO_2-based FE as gate dielectric (DE) is regarded as the most possible solution to reduce power consumption by reducing the subthreshold slope (SS) due to their capability to overcome the Boltzmann limitation of 60 mV/decade at room temperature.

The homogeneous single-domain Landau theory suggests that by connecting an FE in series with standard capacitor, a hysteresis-free stabilized NC state can be obtained in the FE below a critical film thickness [2]. However, most reported NC-FETs show a strong contraction between the SS and hysteresis, in which a small SS (large voltage amplification) is usually accompanied with unexpected hysteresis or frequency dependent behavior [7–12]. The physics underlying this transient NC effect is associated to depolarization field, which leads to the formation of multidomain ferroelectricity that differs from the assumed single-domain case [13]. These results imply that the domain pattern of FE polarization plays a key role in the performance of FE-based devices [14].

At present, probing the magnitudes of local polarization and field along the films presents a challenge [15, 16]. Only the averaged polarization versus the average electric field over the film can be obtained. Thus, details of polarization charge in its spatial and temporal evolution can be used to understand the underlying physics of NC. To date, extensive simulation has been used to study the NC effects and NC-FETs [17–21]. For example, the distribution of FE polarization along the gate length due to the non-uniform electric field along the channel in NC-FET is studied by considering the domain

---

* Corresponding author (email: xyliu@ime.pku.edu.cn)

interaction along the channel direction [19]. However, the distribution of FE polarization normal to the channel direction due to depolarization field and its effect on the performance of NC-FET remain to be explored.

The metal-ferroelectric-insulator-metal (MFIM) system is a suitable prototype to study the NC effect under the depolarization field, given that a dead layer, imperfect electrodes such as semiconductor, and intentional interfacial dielectric layer almost always exist [22]. Using the two-dimensional (2D) phase field model [23, 24], the NC effect in $\mathrm{BaTiO_3}$-based MIFIM system is investigated focusing on the thickness effect [25]. However, the study of polarization dynamics and NC for more promising $\mathrm{HfO_2}$-based FE based on the phase field model is still highly required. More importantly, the extend of the (near) hysteresis-free sub-60 mV/decade with maximum voltage amplification attainable for FE $\mathrm{HfO_2}$ needs to be evaluated.

In this work, polarization evolution in Zr-doped $\mathrm{HfO_2}$ (HZO)-based MFIM structure is comprehensively studied by self-consistently solving the 2D time-dependent Ginzburg-Landau and Poisson equations, in which temporal visualization of local polarization charges and electric fields successfully explains the phase transition of MFIM due to the competition between the negative FE anisotropy energy, domain wall energy and depolarization energy. Furthermore, the design space for stabilized NC based on single- and multi-domain pattern is provided by evaluating the effect of FE and DE properties and operation frequency.

2 Simulation methodology

The free energy density per unit volume of the FE can be written as follows [26]:

$$U_F = \alpha P^2 + \beta P^4 + \gamma P^6 + k(\nabla P)^2/2 - \overline{P}\cdot\overline{E}_F - \varepsilon_0\varepsilon_{\mathrm{Fb}}E_F^2/2. \tag{1}$$

The first three terms are the bulk free energy expressed as the well-known Landau-Ginzburg-Devonshire (LGD) polynomial form as a function of the spontaneous polarization P, where α, β and γ are the ferroelectric anisotropy constants [27]. The fourth term is the gradient energy (i.e., domain wall energy) from the domain formation, where k is the gradient coefficient [10]. The last two terms contribute to the electrostatic energy including the depolarization energy [26], where ε_0 and $\varepsilon_{\mathrm{Fb}}$ are the vacuum permittivity and relative background permittivity of the FE respectively, and E_F is the electric field in the FE given by the sum of depolarization field and applied electric field. Notice that the total polarization in the FE is given by $P_T = P + \varepsilon_0(\varepsilon_{\mathrm{Fb}} - 1)E_F$. Based on the phase field model, time (t)-dependent Ginzburg-Landau (TDGL) equation in 2D domain (x-z coordinate) is written as follows [25]:

$$-\frac{1}{\Gamma}\frac{\mathrm{d}P}{\mathrm{d}t} = 2\alpha P + 4\beta P^3 + 6\gamma P^5 - k\left(\frac{\mathrm{d}^2P}{\mathrm{d}x^2} + \frac{\mathrm{d}^2P}{\mathrm{d}z^2}\right) - E_{F,z}, \tag{2}$$

where Γ is a conductivity of polarization switching.

Figure 1(a) and (b) shows the metal-ferroelectric-metal (MFM) and MFIM structures respectively. To explore domain pattern in the MFIM, 2D electrostatics need to be solved, because the boundary condition at the FE and DE interface is inhomogeneous when multiple domain are considered [21]. The Poisson equation is written as follows:

$$\varepsilon_0\varepsilon_r\nabla^2\varphi = \nabla\cdot\overline{P}, \tag{3}$$

where φ is the electric potential inside the MFIM structure, and ε_r is $\varepsilon_{\mathrm{Fb}}$ and ε_D in the FE and DE respectively. Notice that spontaneous polarization P is zero in the DE.

Then based on the COMSOL multiphysics software, the polarizations and electrostatics of the MFIM structure are self-consistently solved by Poisson and TDGL equations using the periodic boundary conditions to fully investigate the evolution of domain pattern with time or external field for different geometries and material properties. This process is carried out by using a time dependent ramp bias $V_{\mathrm{App}}\sin(2\pi f\cdot t)$ on the top electrode of MFIM structure. Using HZO as FE, Table 1 lists default simulation parameters unless otherwise specified. The fabrication and measurement of HZO capacitor have been described in [28]. Figure 1(c) shows the comparison between the measured and simulated polarization-electric field (P-E) characteristics of MFM capacitor, extracting the FE parameters based on the approach in [28]. Here the first-order phase transition of the FE, where $\alpha <0$, $\beta <0$, and $\gamma >0$, is considered due to the depolarization fields that emerge in the MFIM structure [29].

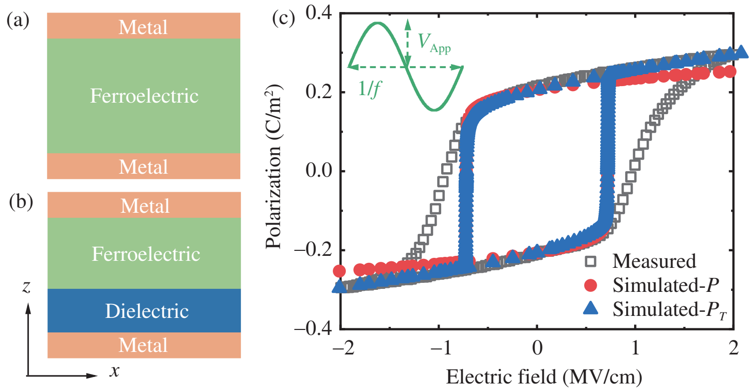

Figure 1 (Color online) (a) MFM and (b) MFIM structures, where top electrode is biased by $V_{\mathrm{App}}\sin(2\pi f\cdot t)$, and bottom electrode is grounded. (c) Measured and simulated P-E characteristics of MFM capacitor with 10 nm HZO film, showing the model calibration. Notice that measured slow switching of FE can be obtained by considering distribution of FE parameters.

Table 1 Default parameters used in the simulation

Symbol	Quantity	Value
α	Landau constant of ferroelectric	-2.9×10^{8} V·m/C
β	Landau constant of ferroelectric	-4.0×10^{8} V·m^5/C^3
γ	Landau constant of ferroelectric	6.0×10^{10} V·m^9/C^5
k	Gradient coefficient of ferroelectric	1×10^{-10} V·m^3/C
Γ	Conductivity of polarization switching	10 S/m
$\varepsilon_{\mathrm{Fb}}$	Dielectric constant of ferroelectric	25
ε_D	Dielectric constant of dielectric	25
T_F	Thickness of ferroelectric	10 nm
T_D	Thickness of dielectric	5 nm
L	Lateral size of simulation region	50 nm
V_{App}	Amplitude of external applied voltage	10 V
f	Sweep frequency of applied voltage	10^6 Hz

3 Results and discussion

3.1 Impact of ferroelectric properties

Figure 2(a)–(f) plots the P-E characteristics of MFIM structure with different FE thickness ($T_F=50$, 40, 30, 15, 5 and 3 nm). The overall P-E curve consists of two components: the FE polarization-FE field (P_F-E_F) and the DE polarization-DE field (P_D-E_D), where the P_F-E_F obtained from the LGD theory is also shown. When T_F is thick, the overall P-E curve of FE-DE stack exhibits remnant polarization and significant hysteresis, which are two important features of the FE as shown in Figure 2(a). As T_F decreases, the remnant polarization in the MFIM structure gradually decreases (Figure 2(b)) and finally disappears (Figure 2(c)). Below this critical thickness, polarization switching of the FE-DE stacks behaves as that of the antiferroelectric (AFE), which has zero remnant polarization and field-induced double hysteresis as shown in Figure 2(d) and (e). When T_F is thinner than another critical thickness, P_F-E_F precisely follows the LGD path (i.e., S-curve) without hysteresis, and the overall P-E curve of MFIM structure acts as that of the paraelectric.

Figure 3(a) shows the critical thicknesses related to the aforementioned phase transition of MFIM structure with various gradient coefficients at the equilibrium state ($V_{\mathrm{App}}=0$). $T_{\mathrm{cri,A}}$ is the critical thickness above which P-E characteristics are always hysteretic with remnant polarization, and $T_{\mathrm{cri,C}}$ is the critical thickness below which P-E characteristics are always hysteresis-free. The region between $T_{\mathrm{cri,A}}$ and $T_{\mathrm{cri,C}}$ is the AFE-like FE-DE stacks. Figure 3(b) shows the domain patterns at $V_{\mathrm{App}}=0$ within three different regions labeled as A, B, and C, which are separated by $T_{\mathrm{cri,A}}$ and $T_{\mathrm{cri,C}}$. In region A, polarization is homogeneous with the overall $P\neq0$, resulting in remnant polarization. This is attributed to the negative FE anisotropy energy that is the dominant part, implying that the depoled state ($P=0$) is unstable. In region B, anti-parallel (strip) domains with $P\uparrow=-P\downarrow\neq0$ will form. This condition reduces the large electrostatic energy due to the depolarization field despite the increase in domain wall

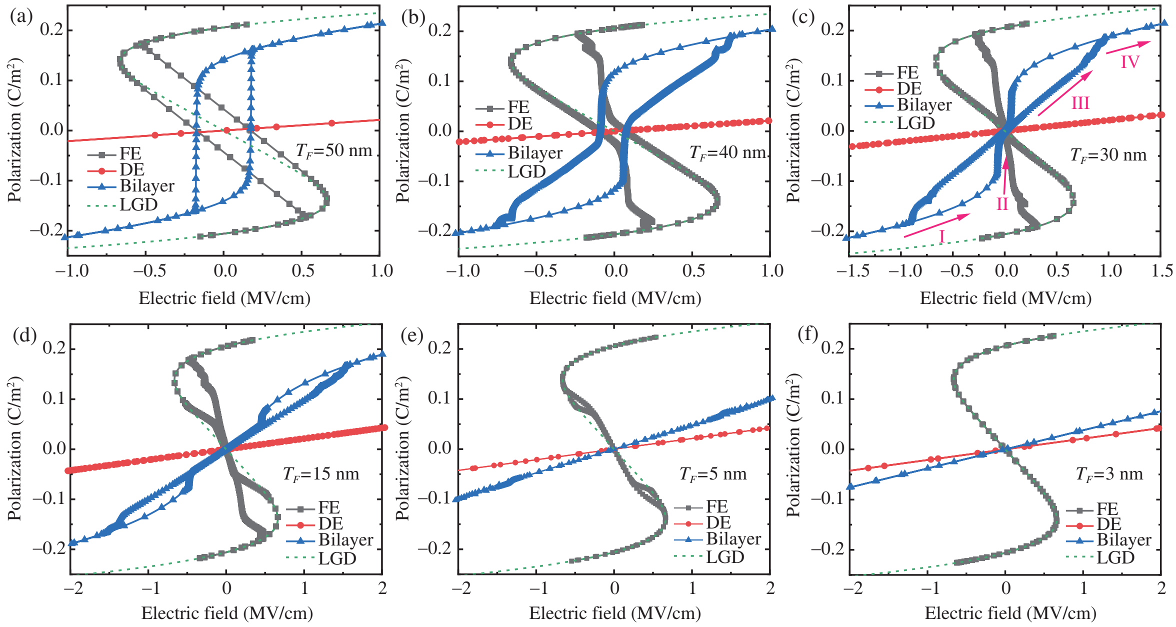

Figure 2 (Color online) P-E characteristics in the MFIM structure with (a) $T_F = 50$ nm, (b) $T_F = 40$ nm, (c) $T_F = 30$ nm, (d) $T_F = 15$ nm, (e) $T_F = 5$ nm, and (f) $T_F = 3$ nm. Black square is the P_F-E_F, red circle is the P_D-E_D, blue triangle is the overall P-E of FE-DE bilayer, green dash is the P_F-E_F based on the LGD theory. All the simulation parameters are from Table 1 except for T_F.

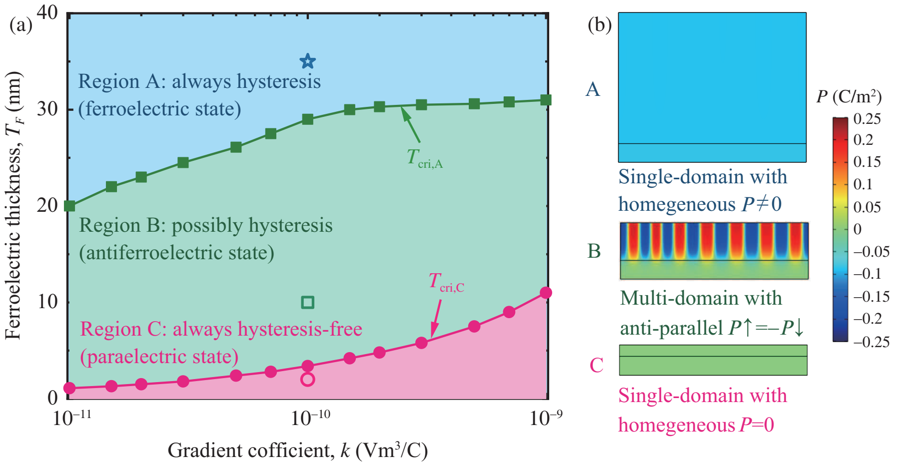

Figure 3 (Color online) (a) Critical ferroelectric thickness $T_{\mathrm{cri,A}}$ and $T_{\mathrm{cri,C}}$ for phase transition of MFIM with various gradient coefficient at equilibrium state ($V_{\mathrm{App}} = 0$). (b) Domain patterns at $V_{\mathrm{App}} = 0$ at the specified T_F in (a) within region A, B and C, respectively.

energy. Accordingly, Figure 4 shows the domain widths and patterns with different FE thicknesses and gradient coefficients in the MFIM in region B. As the T_F decreases, the domain width (W_D) becomes more uniform and narrower. However, when T_F decreases within region C, if such strip domains still exist, the domain period will be more intensive, and the sum of domain wall energy and depolarization energy can be larger than the negative FE anisotropy energy. Thus, polarization transitions into the homogeneously depoled state ($P = 0$) (Figure 3(b)), which is energetically more stable than any other configuration with finite polarization. Additionally, the decrease in gradient coefficient will give rise to the decrease in domain wall energy despite the narrow strip domain. Therefore, a small $T_{\mathrm{cri,C}}$ with high depolarization energy is needed to exceed the FE anisotropy energy to stabilize the FE at the depoled state. Similarly, a smaller $T_{\mathrm{cri,A}}$ will lead to the formation of strip domain. For a range of two orders of magnitude for gradient coefficient k, $T_{\mathrm{cri,A}}$ varies between 1 and 10 nm, and $T_{\mathrm{cri,C}}$ increases from 20 to 30 nm as k increases.

Besides the aforementioned polarization at equilibrium state, the polarization dynamics of the MFIM

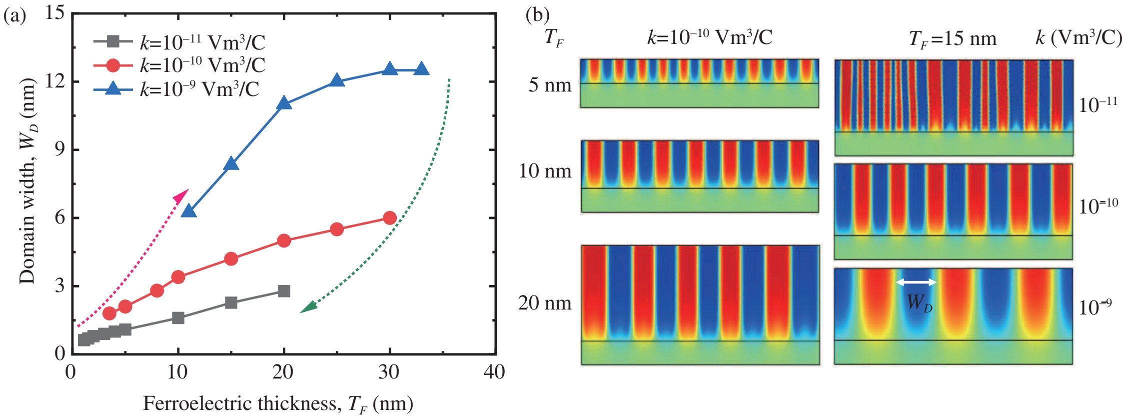

Figure 4 (Color online) (a) Domain width versus ferroelectric thickness with different gradient coefficient at equilibrium state ($V_{\rm App} = 0$) for the region B in Figure 3; (b) domain patterns of MFIM for different T_F and different k at $V_{\rm App} = 0$.

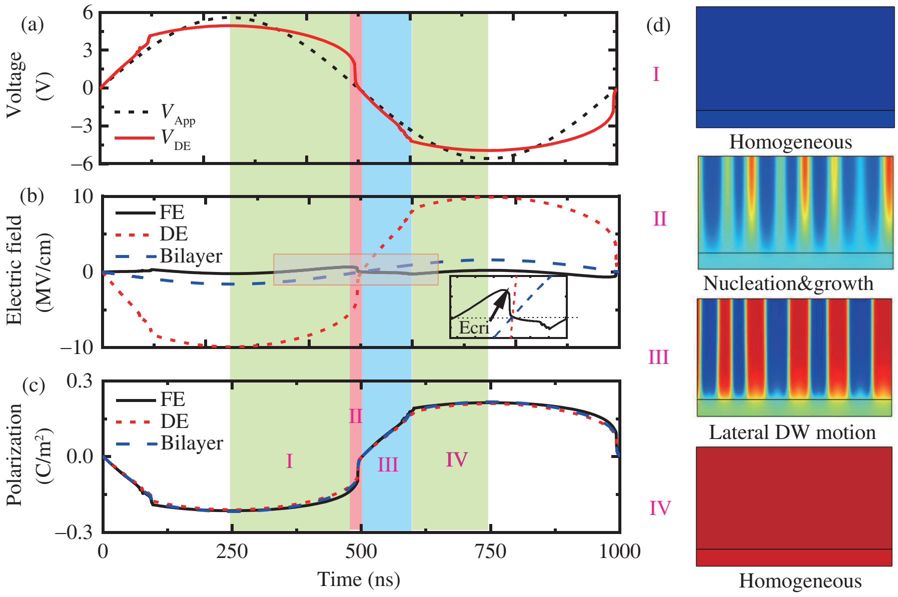

Figure 5 (Color online) (a) Voltages ($V_{\rm DE}$ and $V_{\rm App}$), (b) electric fields, and (c) polarization charges as a function of time in MFIM with $T_F = 30$ nm operated at frequency of 1 MHz as shown in Figure 2(c). (d) Polarization domain patterns from the fully negatively polarized state (downward P_z, blue) to fully positively polarized state (upward P_z, red) corresponding to the stage I, II, III, and IV, respectively.

structure is analyzed. Figure 5 shows the time-dependent voltages of $V_{\rm App}$ and $V_{\rm DE}$ (a), electric fields (b), polarization charges (c), and local polarization profiles (d), where T_F is 30 nm in relation to Figure 2(c). We focus on the switching behavior from the fully negatively polarized state (downward P_z) to the fully positively polarized state (upward P_z). In the stage I, FE polarization is homogeneously changing mainly due to background permittivity of the FE. As $V_{\rm App}$ changes, only the FE field gradually changes from negative (downward) to positive (upward) value that is opposite to the external field, due to the depolarization field. Once FE field reaches the critical field $E_{\rm cri}$ (≈ 0.65 MV/cm), it transitions into the stage II, and switching occurs by reverse domain nucleation and growth. Then, strip domains rapidly fill in the whole film within about 10 ns, leading to the abrupt change in the polarization charges and electric field in FE and DE. This finding confirms that the formation of stripe domain is attributed to the high depolarization field and can effectively reduce the electrostatic energy. The initial nucleation occurs randomly, which is different from [25], where nucleation occurs at the center of the bottom interface because of the predefined defect. In stage III, polarization switching proceeds by lateral motion of the stripe domain, in which one polarized state expands and the other one shrinks. This process lasts for 90 ns until the whole FE film becomes positively polarized state. Interestingly, the change in polarization induced by lateral motion of strip domain is approximately proportional to the time at the fixed domain

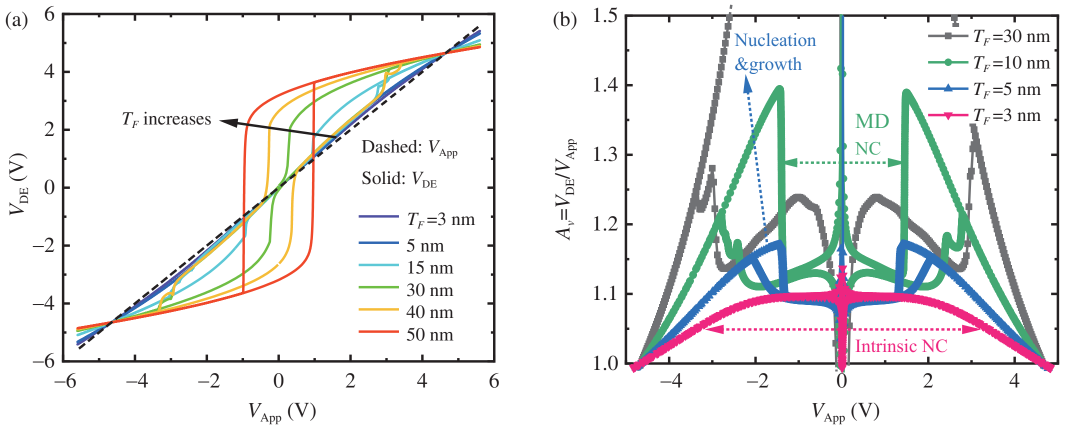

Figure 6 (Color online) (a) V_{DE}-V_{App} and (b) A_v-V_{App} characteristics with different T_F.

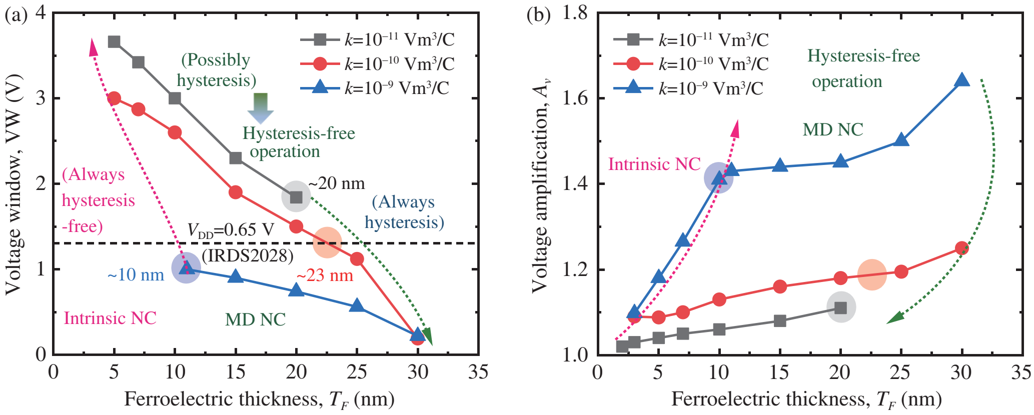

Figure 7 (Color online) (a) Voltage window and (b) voltage amplification factor for hysteresis-free operation versus T_F with different k.

wall velocity ($\sim 4.4\times10^{-2}$ m/s), which is considerably slower than that of the nucleation and growth process. Then, FE switching approaches stage IV, which is similar to stage I. Additionally, from Figure 5(a), voltage amplification on the DE layer is observed when the direction of FE field is opposite to that of the DE field and overall bilayer field. Such opposite changes in the polarization charge and electric field in the FE layer indicate the negative permittivity of FE and the NC effect.

The abovementioned polarization reversal in HZO is similar to that of BaTiO$_3$ [25]. Consistent with [25], the domain nucleation and growth at $\pm E_{\mathrm{cri}}$ always lead to hysteresis. By contrast, the lateral motion of strip domain can be recovered during the reverse sweep, which provides a possible mechanism to obtain hysteresis-free operation. This effect originated from the strip domain is regarded as the multi-domain NC (MD NC). Figure 6(a) shows the V_{DE}-V_{App} in MFIM structure for different T_F corresponding to those in Figure 2. As T_F decreases, the range of hysteresis-free operation by MD NC of P-E and V_{DE}-V_{App} characteristics is extended. When FE film is very thick (Figure 2(a)), polarization reversal instantaneously occurs by nucleation without formation of strip domain in the entire field range. As T_F decreases (Figures 2(b)–(e)), the small V_{App} enables the FE field to reach the E_{cri} and trigger rapid nucleation and growth. The high depolarization field eases the formation of strip domains. Moreover, as T_F becomes thinner and below that of $T_{\mathrm{cri,C}}$ (Figure 2(f)), polarization homogeneously switches in the entire field range due to the extremely high depolarization field, where FE works under intrinsic NC as proposed in [2]. Figure 6(b) indicates that voltage amplification factor A_v ($= V_{\mathrm{DE}}/V_{\mathrm{App}}$) values related to the MC NC are generally lower compared with nucleation and growth, and the A_v of intrinsic NC is very close to that of the MD NC with very thin T_F. If a high voltage ($V_{\mathrm{App}} > 4$ V) is applied to MFIM, FE is in fully polarized state, and behaves as the conventional DE with neither NC nor voltage amplification. Still, voltage amplification can be enhanced by further optimization which will be addressed in the following section.

Figure 7(a) and (b) shows the voltage window (VW) and A_v for hysteresis-free operation versus FE

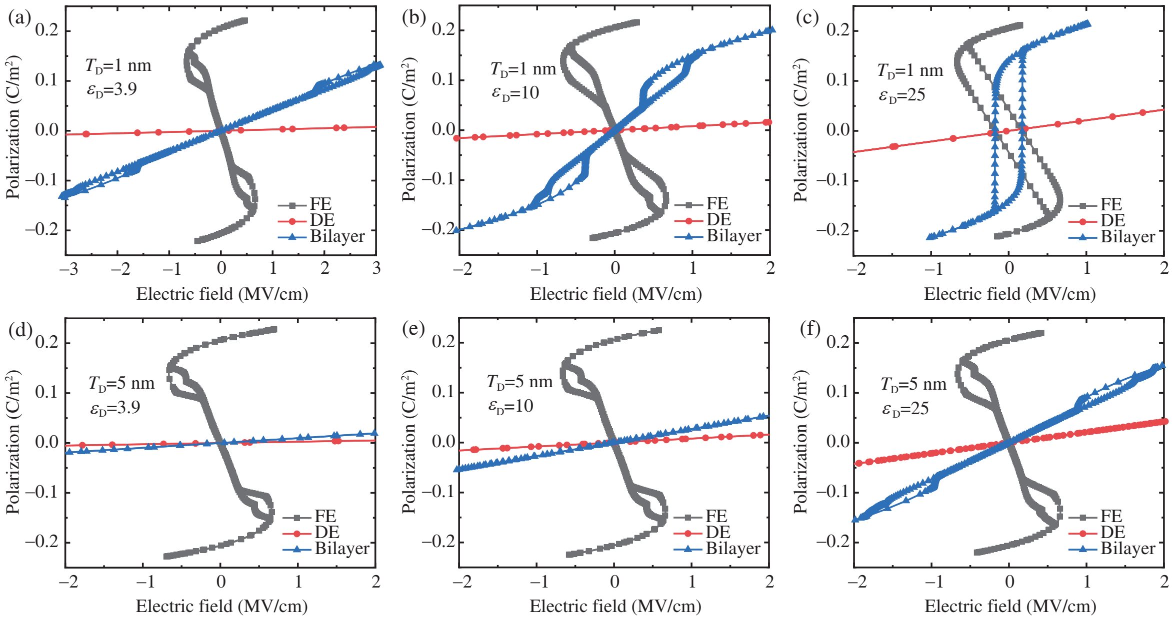

Figure 8 (Color online) P-E characteristics in the MFIM structure with different T_D and ε_D, accounting for SiO$_2$, Al$_2$O$_3$, and HfO$_2$, respectively. (a)–(c) and (d)–(f) are the $T_D = 1$ nm and 5 nm cases. All the simulation parameters are taken from Table 1 except for T_D and ε_D.

thickness with different gradient coefficients. In terms of VW, only T_F in region B needs to be explored, as FEs thinner or thicker beyond this region are either always hysteresis-free or always hysteretic. In terms of A_v, T_F in region C is also considered. As T_F decreases or k decreases in the MFIM, which is generally accompanied by a small domain size (Figure 4), VW increases, but voltage boosting is weakened. For example, in the case of $k = 10^{-10}$ V·m^3/C, as T_F changes from 30 to 3 nm, W_D decreases from 6 to 1.5 nm, VW increases from 0.2 to 3 V, but A_v decreases from 1.2 to 1.1. As a result, optimization of the T_F is required to obtain the sufficient VW and the voltage amplification as large as possible. Here, power supply voltage $V_{\rm DD}$ of 0.65 V is considered in accordance with the IRDS requirement1). In the low k case (10^{-11} V·m^3/C), the VW is always larger than 2$V_{\rm DD}$. Thus, a high T_F is preferred to improve A_v but it is limited to below $T_{\rm cri,A}$ (∼20 nm), because remnant polarization occurs beyond this thickness. In the moderate k case (10^{-10} V·m^3/C), the optimal T_F is ∼23 nm, where VW satisfies the $V_{\rm DD}$ requirement along with high A_v (∼1.2). In the high k case (10^{-9} V·m^3/C), the VW operated in region B is always lower than 2$V_{\rm DD}$ despite their large A_v. Under this condition, T_F in MFIM should be designed always in the hysteresis-free range by thinning the T_F below $T_{\rm cri,C}$ (∼10 nm) and as close to $T_{\rm cri,C}$ as possible to improve A_v (∼1.4).

3.2 Impact of dielectric properties

It is claimed that domain wall motion based NC path in FE is independent of T_D but depends on the permittivity of the DE layer [30]. However, our simulation implies that the effect of DE property on polarization switching in the MFIM is determined by the equivalent oxide thickness (EOT) (i.e., DE capacitance C_D) related to ε_D/T_D, as discussed in the following. Figure 8 shows the P-E characteristics in the MFIM structure with T_D of 1 and 5 nm, taking SiO$_2$, Al$_2$O$_3$, and HfO$_2$ as examples. First, in the $T_D = 1$ nm case, high ε_D has significant impact not only on the P_D-E_D but also the P_F-E_F characteristics. Second, in the $\varepsilon_D = 25$ case, thin T_D has similar impact as high DE permittivity. A high permittivity and/or thin thickness of DE will effectively reduce the DE field and enhance the FE field, indicating a reduction of depolarization field in the FE layer, which is consistent with $E_{\rm Dep} = P[\varepsilon_0\varepsilon_{\rm Fb}(C_D/C_F + 1)]^{-1}$ [1]. Consequently, the case having the highest ε_D/T_D in Figure 8(c) is notably distinguished from others due to its considerably small depolarization field, whose effect is equivalent to the thick T_F as shown in Figure 2(a).

Next, we examine the interdependence of polarization switching on the ε_D and T_D. Figure 9 shows the P-E and $V_{\rm DE}$-$V_{\rm App}$ characteristics with different ratios of ε_D/T_D by proportionally changing the

---

1) International Roadmap for Devices and Systems. 2018. https://irds.ieee.org/.

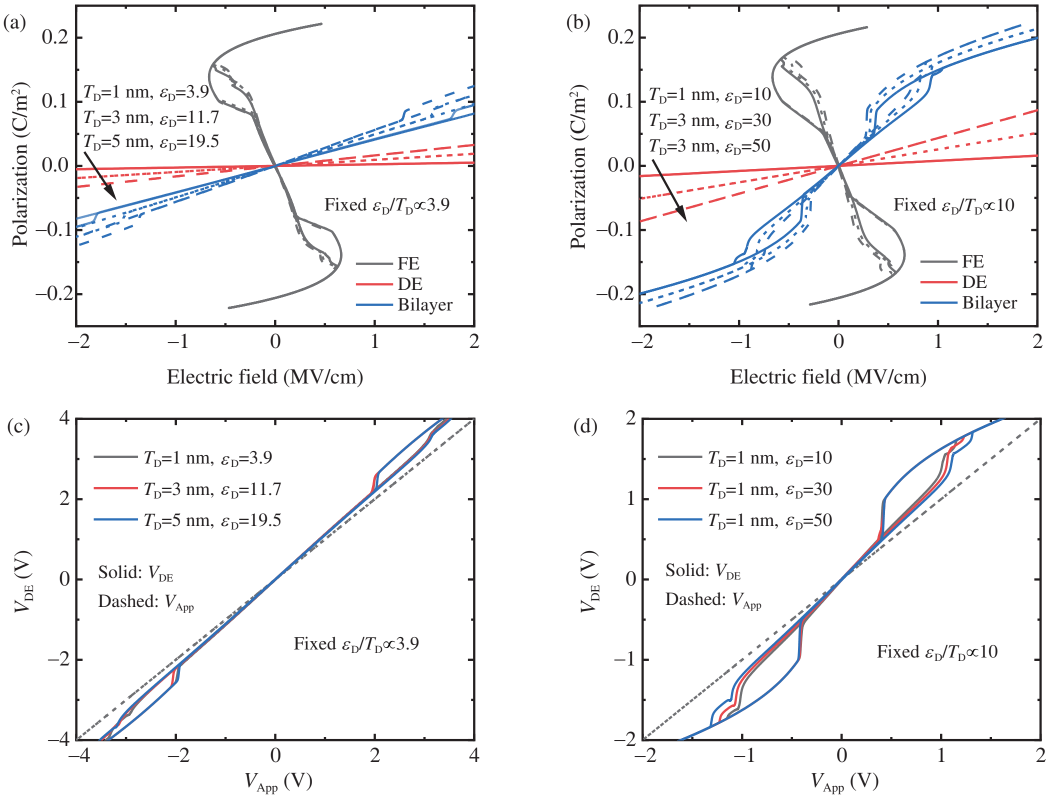

Figure 9 (Color online) (a), (b) P-E and (c), (d) $V_{\rm DE}$-$V_{\rm App}$ characteristics in the MFIM structure with different values of ε_D/T_D respectively. (a), (c) are the $\varepsilon_D/T_D\propto$ 3.9 cases, and (b), (d) are the $\varepsilon_D/T_D\propto$ 10 cases.

ε_D with T_D. Under the fixed ratio of ε_D/T_D, the slope of P_D-E_D changes with ε_D. However, P_F-E_F and the resultant $V_{\rm DE}$-$V_{\rm App}$ are almost coincident with each other especially under low ε_D/T_D due to their almost the same depolarization field. Therefore, polarization switching is dependent on the ratio of ε_D/T_D by modulating the depolarization field in FE. With respect to hysteresis-free operation, a low ε_D/T_D provides a large VW but small voltage amplification, where MD NC works due to the high depolarization field.

3.3 Impact of operation frequency

Figure 10 shows the P-E characteristics of the MFIM structure with different conductivities (Figure 10(a)–(c)) and operation frequencies (Figure 10(d)–(f)). When voltage drive speed is lower than the domain wall motion speed, the MFIM shows hysteresis-free intrinsic NC behavior as shown in Figure 10(d). Particularly, as frequency varies, negligible difference is observed in terms of the domain width W_D, which is determined by the competition between the negative FE energy, domain wall energy, and depolarization energy as mentioned in Subsection 3.1. However, as f increases, or Γ decreases, no formation of strip domain motion appears, and hysteresis occurs due to large delay. The switching of hysteretic P-E in Figure 10(b) and (f) (smoother) is different from those in Figures 2(a) and 7(c) (more abrupt). Particularly, critical field $E_{\rm cri}$ is dependent on Γ and f but is independent of T_F, k, and ε_D/T_D (Figures 2 and 7).

Figure 11 shows the related (a) VW and (b) voltage amplification factor. For the hysteresis-free operation in the MD NC regime, as f increases, VW significantly decreases, and A_v slightly decreases. Additionally, an upper limit of frequency beyond which MFIM system operates in always hysteretic range exists. This limit depends on the value of conductivity, which plays an important role in polarization switching. The experimentally extracted value of Γ for FE HZO is estimated to be generally smaller than 0.01 S/m [25]. Given the $V_{\rm DD}$ requirement, the maximum frequency for 10 S/m case is at approximately the megahertz scale. Therefore, enabling an FE HZO suitable for steep-slope devices applied to high-speed circuit up to gigahertz frequency needs a considerably amount of conductivity. According to our calculation, the conductivity Γ should be at least 500 S/m to obtain the hysteresis-free operation at the

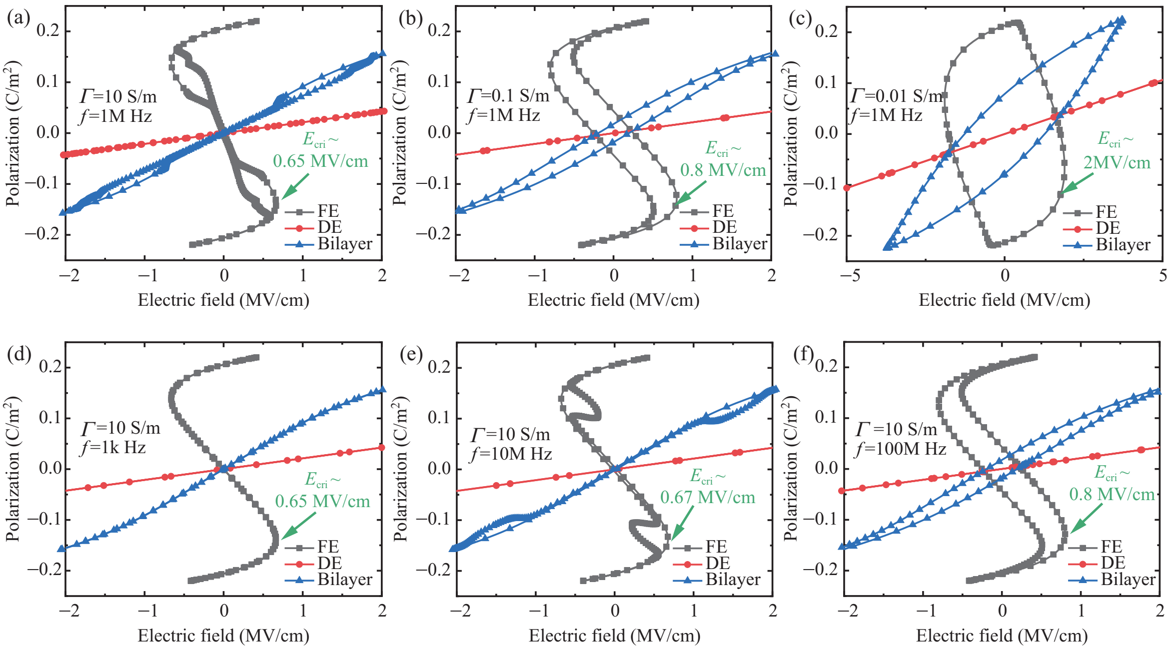

Figure 10 (Color online) (a)–(c) *P*-*E* characteristics in the MFIM structure with different conductivity (Γ = 10, 0.1 and 0.01 S/m) operated at f = 1M Hz. (d)–(f) *P*-*E* characteristics with Γ = 10 S/m operated at f = 1k, 10M and 100M Hz. All the simulation parameters are taken from Table 1 except for Γ and f.

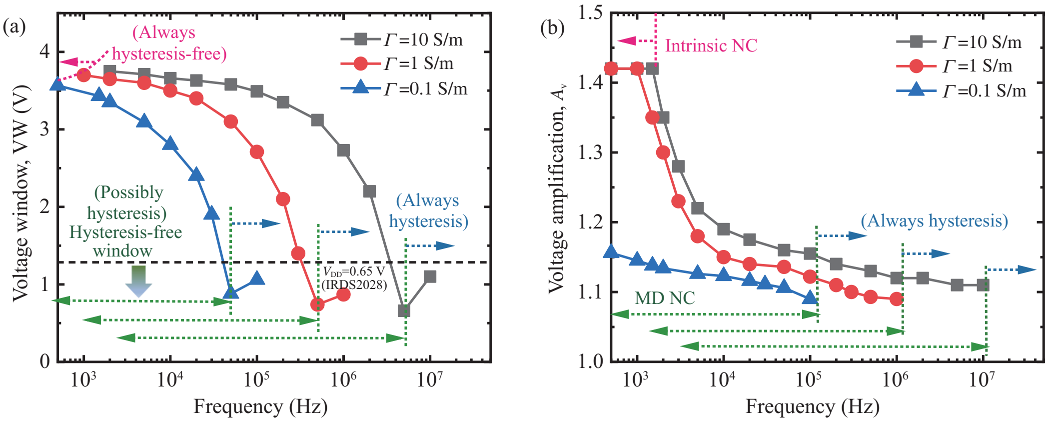

Figure 11 (Color online) (a) Voltage window and (b) voltage amplification for hysteresis-free operation versus frequency with different Γ.

overall electric field.

4 Conclusion

Electrically induced phase transition in the MFIM with different domain patterns (homogeneous versus strip domain) occurs at two critical thicknesses from the single loop of ferroelectric to double loops of antiferroelectric and eventually to the linear line of paraelectric due to the depolarization field in FE. The design space for stabilized negative capacitance (both intrinsic NC and MD NC) with (near) hysteresis-free operation together with voltage amplification in the MFIM structure depends on the capacitance matching between FE and DE via adjusting the FE thickness, gradient coefficient, DE thickness, and permittivity, and depends on the operation frequency. Particularly, satisfying the $V_{\rm DD}$ requirement, HZO based MFIM with T_F of several nanometers and DE EOT less than 1 nm theoretically possesses A_v around 1.1∼1.4, implying that hysteresis-free SS decreases to 42∼54 mV/decade, thus limiting the megahertz sweep frequency for NC-FET. Polarization dynamics based on phase field model provide physical insights, which are helpful in the design and optimization of steep-slope NC devices and nonvolatile memory devices based on HfO_2-based FEs.

Acknowledgements This work was supported in part by National Natural Science Foundation of China (Grant Nos. 61804003, 61674008) and in part by China Postdoctoral Science Foundation (Grant Nos. 2019T120017, 2018M630034).

References

1 Hoffman J, Pan X, Reiner J W, et al. Ferroelectric field effect transistors for memory applications. Adv Mater, 2010, 22: 2957–2961

2 Salahuddin S, Datta S. Use of negative capacitance to provide voltage amplification for low power nanoscale devices. Nano Lett, 2008, 8: 405–410

3 Yang H, Xiao M Q, Cui Y, et al. Nonvolatile memristor based on heterostructure of 2D room-temperature ferroelectric α-In_2Se_3 and WSe_2. Sci China Inf Sci, 2019, 62: 220404

4 Böscke T S, Müller J, Bräuhaus D, et al. Ferroelectricity in hafnium oxide thin films. Appl Phys Lett, 2011, 99: 102903

5 Wang L F, Luo Y, Wang J S, et al. Temperature-dependent evolution of surface charge screening and polarization at ferroelectric surfaces. Sci China-Phys Mech Astron, 2019, 62: 987721

6 Zhang H, Long W J, Chen Y Q, et al. Enhanced electrical properties in bilayered ferroelectric thin films. Sci China-Phys Mech Astron, 2013, 56: 551–555

7 Khan A I, Chatterjee K, Duarte J P, et al. Negative capacitance in short-channel FinFETs externally connected to an epitaxial ferroelectric capacitor. IEEE Electron Device Lett, 2016, 37: 111–114

8 Zhou J R, Han G Q, Li Q L, et al. Ferroelectric $HfZrO_x$ Ge and GeSn PMOSFETs with Sub-60 mV/decade subthreshold swing, negligible hysteresis, and improved I_{DS}. In: Proceedings of IEEE International Electron Devices Meeting (IEDM), San Francisco, 2016. 310–313

9 Wang H M, Huang Q Q, Yang M X, et al. Deep insight into the voltage amplification effect from ferroelectric negative capacitance. Sci China Inf Sci, 2019, 62: 089401

10 Zhou J R, Han G Q, Xu N, et al. Incomplete dipoles flipping produced near hysteresis-free negative capacitance transistors. IEEE Electron Device Lett, 2019, 40: 329–332

11 Zhou J R, Han G Q, Li J, et al. Negative differential resistance in negative capacitance FETs. IEEE Electron Device Lett, 2018, 39: 622–625

12 Zhou J R, Han G Q, Li J, et al. Comparative study of negative capacitance Ge pFETs with $HfZrO_x$ partially and fully covering gate region. IEEE Trans Electron Device, 2017, 64: 4838–4843

13 Hoffmann M, Pešić M, Slesazeck S, et al. On the stabilization of ferroelectric negative capacitance in nanoscale devices. Nanoscale, 2018, 10: 10891–10899

14 Jin C J, Jang K, Saraya T, et al. Experimental study on the role of polarization switching in subthreshold characteristics of HfO_2-based ferroelectric and anti-ferroelectric FET. In: Proceedings of IEEE International Electron Devices Meeting (IEDM), San Francisco, 2018. 723–726

15 Kalinin S V, Morozovska A N, Chen L Q, et al. Local polarization dynamics in ferroelectric materials. Rep Prog Phys, 2010, 73: 056502

16 Zubko P, Stucki N, Lichtensteiger C, et al. X-ray diffraction studies of 180° ferroelectric domains in $PbTiO_3/SrTiO_3$ superlattice under an applied electric field. Phys Rev Lett, 2010, 104: 187601

17 You W X, Su P. Intrinsic difference between 2-D negative-capacitance FETs with semiconductor-on-insulator and double-gate structures. IEEE Trans Electron Device, 2018, 65: 4196–4201

18 Rollo T, Wang H, Han G, et al. A simulation based study of NC-FETs design: off-state versus on-state perspective. In: Proceedings of IEEE International Electron Devices Meeting (IEDM), San Francisco, 2018. 213–216

19 Saha A K, Sharma P, Dabo I, et al. Ferroelectric transistor model based on self-consistent solution of 2D Poisson's, non-equilibrium Green's function and multi-domain Landau Khalatnikov equations. In: Proceedings of IEEE International Electron Devices Meeting (IEDM), San Francisco, 2017. 326–329

20 Xiao Y G, Tang M H, Li J C, et al. Temperature effect on electrical characteristics of negative capacitance ferroelectric field-effect transistors. Appl Phys Lett, 2012, 100: 083508

21 Ota H, Ikegami T, Hattori J, et al. Fully coupled 3-D device simulation of negative capacitance FinFETs for sub 10 nm integration. In: Proceedings of IEEE International Electron Devices Meeting (IEDM), San Francisco, 2016. 318–321

22 Mehta R R, Silverman B D, Jacobs J T. Depolarization fields in thin ferroelectric films. J Appl Phys, 1973, 44: 3379–3385

23 Stephanovich V A, Luk'yanchuk I A, Karkut M G. Domain-enhanced interlayer coupling in ferroelectric/paraelectric superlattices. Phys Rev Lett, 2005, 94: 047601

24 Zhou G Z, Wang Y X, Liu C, et al. On ferroelectric domain polarization switching mechanism subject to an external electric field by simulations with the phase-field method. Sci China Tech Sci, 2013, 56: 1129–1138

25 Park H W, Roh J, Lee Y B, et al. Modeling of negative capacitance in ferroelectric thin films. Adv Mater, 2019, 8: 1805266

26 Woo C H, Zheng Y. Depolarization in modeling nano-scale ferroelectrics using the Landau free energy functional. Appl Phys A, 2008, 91: 59–63

27 Devonshire A F. Theory of barium titanate. Philos Mag J Sci, 1949, 40: 1040–1063

28 Chang P Y, Zhang Y Z, Du G, et al. Experiment and modeling of dynamical hysteresis in thin film ferroelectrics. Jpn J Appl Phys, 2020, 59: 7

29 Batra I P, Wurfel P, Silverman B D. Phase transition, stability, and depolarization field in ferroelectric thin films. Phys Rev B, 1973, 8: 3257–3265

30 Cano A, Jiménez D. Multidomain ferroelectricity as a limiting factor for voltage amplification in ferroelectric field-effect transistors. Appl Phys Lett, 2010, 97: 133509